buildings

MDPI

Article

Modeling and Seismic Performance Analysis of Grid Shear Walls

Weijing Zhang *, Caiwang Li and Xiao Chu

College of Architecture and Civil Engineering, Beijing University of Technology, Beijing 100124, China; licwnm@163.com (C.L.); chuxiaoo@sina.com (X.C.)
* Correspondence: zhangweijing@bjut.edu.cn

Abstract: Prefabricated insulation grid shear walls are a new type of wall which integrates structure, insulation and formwork. A grid-like reinforced concrete shear wall with vertical and transverse limbs is formed by casting concrete into the reserved vertical and transverse hollow cavities in the prefabrication of cement polystyrene granular concrete wall formworks. In this paper, based on an earthquake engineering simulation open system (OpenSees), a new modeling approach for grid shear walls is proposed, and nonlinear analysis of two grid walls with different grid sizes under cyclic load is carried out. The accuracy and effectiveness of the grid shear wall model are verified by comparison of the predicted hysteretic response and experimental results. On this basis, the seismic performance of grid shear walls with different parameters (axial load ratio, vertical reinforcement ratio, transverse reinforcement ratio and transverse limb height) is analyzed. The results show that both axial load ratio and vertical reinforcement ratio can significantly improve the load capacity of grid shear walls. However, with an increase in the axial load ratio, the ductility of the grid shear walls decreases. The influence of transverse reinforcement ratio and transverse limb height on the load capacity of shear wall with large shear span ratio is relatively small, mainly because the failure mode of shear wall with large shear span ratio is bending failure. Based on parameter influence analysis, design suggestions for reinforcement ratio in vertical and horizontal limbs and the height of the transverse limb of grid shear walls are put forward. The research in this paper provides a reference for the application of grid shear walls in engineering.

Keywords: grid shear wall; seismic performance; modeling; OpenSees; parametric analysis

Academic Editor: Tadeh Zirakian

Received: 2 December 2024
Revised: 15 January 2025
Accepted: 17 January 2025
Published: 20 January 2025

Citation: Zhang, W.; Li, C.; Chu, X. Modeling and Seismic Performance Analysis of Grid Shear Walls. *Buildings* **2025**, *15*, 294. https://doi.org/10.3390/buildings15020294

1. Introduction

Cast-in-place concrete bearing wall construction system with formwork insulation integration and no removal formwork has been researched and applied all over the world [1–4]. The main feature of a prefabricated thermal insulation structure is the integration of thermal insulation with load-carrying and formwork. Through the analysis of various systems of formwork and insulation integration, an insulation block formwork cast-in-place reinforced concrete grid shear wall bearing system has been proposed in China. On this basis, to improve construction efficiency, wall formwork is used instead of block formwork. The precast walls are made of cement polystyrene and granular light concrete and are processed in a factory. During construction, steel mesh pieces are inserted into the vertical and transverse through cavity reserved for the wall panel, and concrete is poured to make the middle of the wall a grid-like reinforced concrete shear wall with vertical and transverse limbs as the main force parts (hereinafter referred to as the grid shear wall). Reinforced concrete grid shear walls with insulation formwork offer several advantages, such as eliminating the need for dismantling the formwork and providing insulation, thermal insulation and fire

prevention features. The insulated wall mold grid shear wall system is suitable for seismic and non-seismic medium and tall building structures and has broad application prospects.

The stress system of a prefabricated insulation wall-type grid shear wall is the grid shear wall in the middle part. Some experimental studies have been carried out on the seismic performance of grid shear walls. Wang [5] conducted quasi-static tests on eight grid walls with different shear span ratios and axial load tests on three grid walls. The study concluded that the bearing capacity of a grid shear wall can be calculated according to current specifications. Zhang [6,7] performed quasi-static tests on four grid shear wall specimens with different shear span ratios. The results revealed local compression failure of the concrete at the bottom of the vertical limbs on both sides of the specimens, and vertical cracks appeared at both ends of most of the transverse limbs, indicating that the grid shear wall had good energy dissipation ability. Zhang [8] conducted quasi-static tests on two grid shear walls with small shear span ratios and different grid spacing. This research focused on developing an equivalent thickness calculation method suitable for grid shear walls with different spacing configurations. Dusicka [9,10] focused on the effects of the aspect ratio and vertical load on the seismic performance of grid walls. The results demonstrated that the presence of a vertical load enhanced the lateral bearing capacity of the wall, while the aspect ratio affected the sliding resistance and ductility of the wall. Asadi [11] utilized the finite element software ABAQUS 6.12 to conduct a comprehensive analysis of the grid shear wall test. The research results highlighted the good ductility of insulated grid shear walls, and the reduction coefficient of the wall was determined. Lopez [12] investigated the effect of vertical and longitudinal reinforcement ratios on the seismic performance of insulated grid shear walls.

Numerical analysis is a widely used method for studying the seismic performance of structural members. The nonlinear modeling of RC structural walls is an especially hot topic [13]. Various modeling approaches and finite element software can be used to model structural walls [14,15]. To accurately capture the characteristics of a wall, solid elements are used by many researchers. Xu [16] utilized the finite element software MSC.Marc with solid elements to develop a finite element model of prefabricated reinforced concrete shear walls. Compared to the phenomena observed in the experiment, the finite element model effectively captured the strength, stiffness and significant damage. Wang [17] performed numerical analysis on steel-plate shear walls using ABAQUS finite element software with solid elements and introduced a novel concrete triaxial constitutive model. The analysis results exhibited strong concordance with the experimental data. Jothimani [18] employed ANSYS finite element software with solid elements to simulate the cyclic loading of RC shear walls, validating the accuracy of the finite element model. Zhang [19] employed solid elements and MSC.Marc software to study the cyclic behavior of prefabricated hollow shear walls, aiming to validate the reliability of the finite element model.

Although solid modeling can accurately obtain the mechanical performance of components, the disadvantage is that the modeling is complicated and requires more computing power and time. In recent years, an open system for earthquake engineering simulation (OpenSees, [20]) stands out due to its superior computational efficiency and accuracy. OpenSees is an open-source software which incorporates numerous elements, materials models and solution strategies. Petracca [21] employed 2D-plane stress continuous elements to model masonry shear walls and introduced a continuous micro-analysis model for masonry walls based on damage mechanics. The finite element calculation results had good agreement with the experimental results. Olabi [22] simulated steel-plate composite shear walls using fiber beam column elements in the OpenSees platform, and the simulation results exhibited good agreement with the experimental data. Subsequently, parameterized research was conducted. Kolozvari [23] proposed the MVLEM-3D model

to simulate reinforced concrete walls using OpenSees. This model is characterized by its high numerical stability and computational efficiency, and its simulation results have been found to be in good agreement with experimental data. Kolozvari [24,25] made further enhancements to the SFI-MVLEM model, which effectively captures the interaction between axial bending and shear behavior in reinforced concrete walls. Zhang [26] and Rojas [27] performed nonlinear finite element analysis on T-shaped shear walls using fiber beam column elements and layered shell elements in OpenSees, respectively. The findings indicated that the finite element analysis results aligned well with the experimental data. Nakamura [28] analyzed the experimental results of reinforced concrete shear walls under cyclic loading using layered shell elements, estimating the degree of damage to the shear walls from the perspective of energy consumption. Pozza [29] used truss elements to simulate wooden shear walls and evaluated their mechanical performance under earthquake action through numerical simulation. Alvarez [30] simplified the calculation of shear walls by equating them to truss members and analyzed the stress behavior of shear walls using truss elements in OpenSees, effectively capturing the mechanical behavior of shear walls in different stages. Lu [31] improved the existing three-dimensional truss model, validating its reliability through quasi-static tests of shear walls, accurately reflecting the failure state of shear walls. Feng [32] utilized fiber elements and layered shell elements to model beams and plates, and effectively verified the proposed model by comparing its results with the test results of typical beam plates.

Grid shear walls are a new type of wall, and research on their seismic performance is lacking at present. The existing research mainly focuses on experimental research, but the number of specimens is limited, and their seismic performance needs to be further studied by numerical simulation. For numerical simulation, firstly, a grid shear wall model should be proposed. Compared with ordinary solid concrete shear walls, modeling grid shear walls is more complicated because grid shear walls contain transverse limbs, vertical limbs, EPS concrete blocks, etc. So far, there is no efficient and accurate finite element model of grid shear walls. In addition, the research on the effect of different parameters on the seismic performance of grid shear walls is also significantly lacking. In this paper, based on the OpenSees 3.3 software, a new grid shear wall model combining layered shell elements and truss elements is proposed, and finite element analysis on two grid shear wall specimens with different grid sizes and large shear span ratios is conducted. The reliability of the finite element model is verified by comparing the displacement–force relationship curves obtained by finite element analysis with the experimental results. On this basis, the influence of different parameters on the seismic performance of grid shear walls is analyzed, and some useful suggestions are put forward for the design of slender grid shear walls. The research results of this paper provide a reference for the practical application of grid shear walls in engineering.

2. Specimen Program

A thermal insulation wall formwork grid shear wall was developed on the basis of thermal insulation block grid shear wall. The thermal insulation block grid shear wall is made with lightweight thermal insulation hollow building molds, which are made of polystyrene granular concrete (EPS concrete) and has an excellent thermal insulation performance and good mechanical properties. The block mold was prefabricated in a factory and laid on the spot where the wall was to be built. The holes and joints constituted the formwork of the cast-in-place wall. Steel mesh pieces were placed in the horizontal groove of each layer of building, and vertical steel mesh pieces were inserted in the vertical hole, as shown in Figure 1. Concrete was poured into the grid cavity formed by the vertical hole to form a grid concrete wall composed of vertical limbs and transverse limbs. The

construction process of the thermal insulation block formwork grid shear wall is relatively complicated, and the assembly efficiency is low, which cannot meet the requirements for construction speed. Therefore, a wall mold was developed, which replaced the block mold. The resulting grid shear wall developed from the thermal insulation wall mold is shown in Figure 2, which specifically shows the transverse and vertical limbs, EPS concrete blocks between the vertical and transverse limbs, external wall thermal insulation formwork and transverse and vertical reinforcement mesh. Relevant experimental studies have shown that the outer EPS concrete wall mold has little influence on the bearing capacity of grid shear walls [6]. In order to facilitate the observation of the failure phenomenon of the grid wall during the test, the outer EPS concrete wall mold was not included in the test specimen, and only the EPS block between the transverse and vertical limbs of the grid wall was retained.

Figure 1. Grid shear wall with insulated masonry.

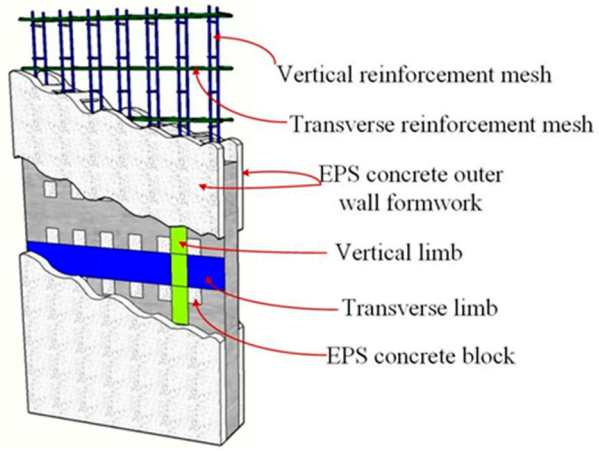

Figure 2. Diagram of grid shear wall.

Two grid shear wall specimens, as detailed in reference [33], were selected to conduct nonlinear finite element modeling of the cyclic response of the grid shear walls. The dimensions of the grid shear wall specimens were 1400 × 2600 mm (length × height), the thickness was 200 mm, the shear span ratio was 1.96, the design axial load ratio was 0.15, and the concrete design strength grade of the wall was C40. Two specimens, W1 and W2, with different grid sizes of 300 × 200 mm and 300 × 300 mm (transverse limb centerline spacing × vertical limb centerline spacing) were analyzed. Additionally, the EPS concrete blocks within the grid shear wall measured 90 × 100 × 200 mm (length × height × thickness). Table 1 outlines the primary parameters of the specimens, where P is the axial load. Figure 3 depicts the dimensions and reinforcement details of the specimens. The steel reinforcement with a strength level of HRB400 was used in specimens, which is noted by the symbol D.

Table 1. Design parameters of grid shear wall specimens.

Specimen ID	Aspect Ratio	Centerline Spacing of Transverse Limbs (mm)	Centerline Spacing of Vertical Limb (mm)	Transverse Limb Height (mm)	Vertical Limb Length (mm)	*P* (kN)
W1	1.96	300	200	200	110	490
W2	1.96	300	300	200	210	600

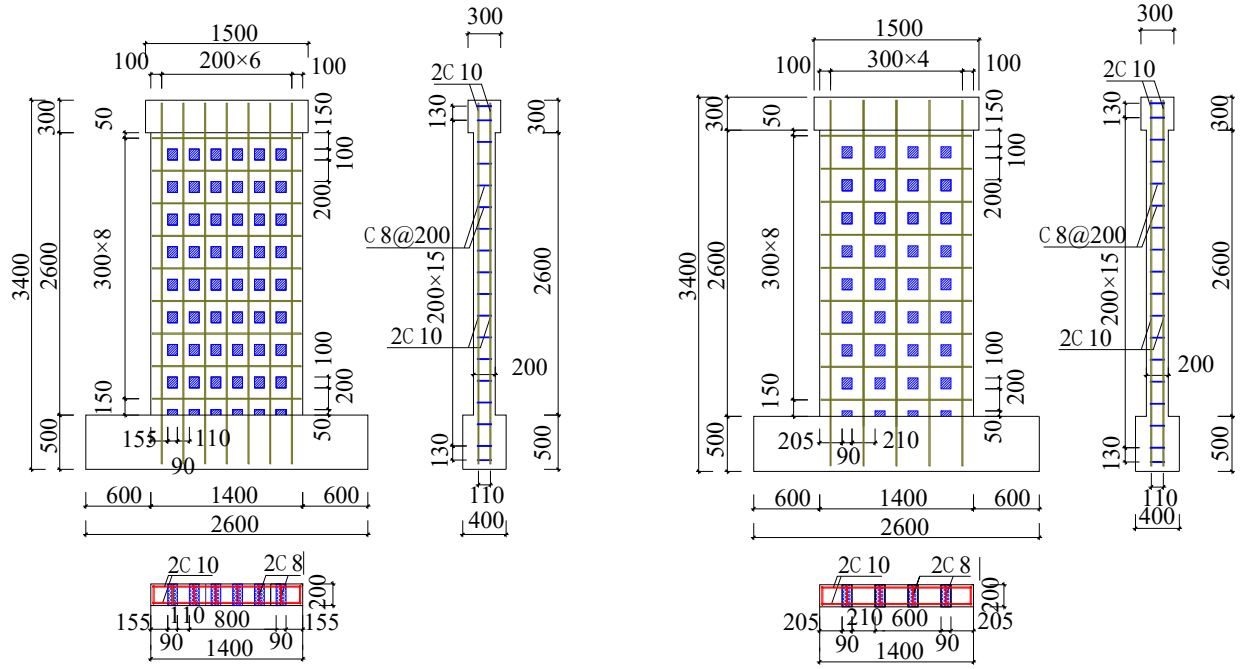

(**a**) W1 (**b**) W2

Figure 3. Dimensions and reinforcement of specimens.

The setup of the specimens is shown in Figure 4. A constant axial load was first applied, and then the cyclic lateral load was applied, and the height of the lateral loading point was 2750 mm above the base of the wall. Force-controlled loading was used, followed by displacement-controlled loading. During the force-controlled stage, 50 kN and 100 kN were used, respectively, and each level was cycled once. During the displacement-controlled stage, the control drift ratio was 0.5% (13.8 mm), 0.75% (20.6 mm), 1.0% (27.5 mm) and then 1.5% (41.2 mm), i.e., each displacement level was repeated for three cycles. The test ended when the lateral force dropped below 85% of the peak load or the specimen could no longer withstand the predetermined axial load.

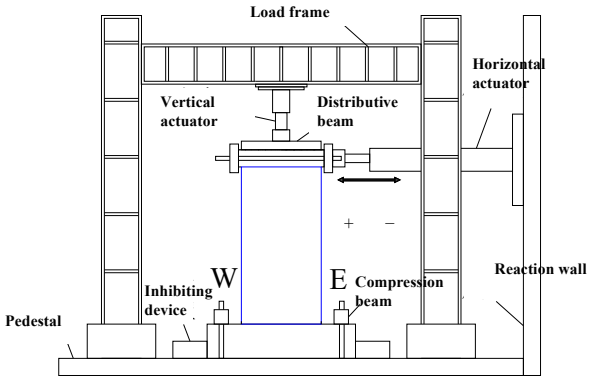

Figure 4. Test setup.

3. Modeling of Grid Shear Walls

The grid shear walls were simulated using OpenSees with the Scientific ToolKit for OpenSees (STKO) [34]. The main modeling procedure included defining nodes, defining elements, defining materials, and defining constraints and analysis. The definitions of nodes, elements, materials and boundary conditions for specimen W1 are introduced in the following sections, and the modeling method for other specimens was similar.

3.1. Defining Nodes

All specimens were 3D models with 6 degrees of freedom per node. Grid wall specimen W1 was divided into six sections along the wall length direction and nine uniform sections along the wall height direction. In the length direction, the length of the two sides of the sections was 300 mm, and the length of middle sections was 200 mm. The nodes and mesh of the model are shown in Figure 5.

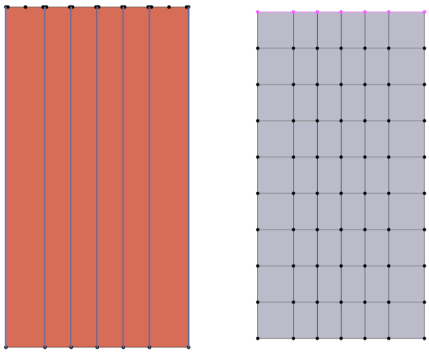

(**a**) Geometry of model (**b**) Mesh of model

Figure 5. Nodes and mesh of the model.

3.2. Element Types

A combined model with truss elements and shell elements was proposed for the grid shear walls.

3.2.1. Truss Element

Discrete truss elements were used to model the vertical bars in the vertical limb of the grid shear wall. According to the principle of area equivalence, two vertical steel bars (each 10 mm in diameter) in the vertical limb were considered to be equivalent to one vertical steel bar. The adjacent vertical nodes in Figure 5 were defined as the truss element. In the process of modeling, the joint force between the truss element and the shell element was realized through the shared node.

3.2.2. Layered Shell Element

Based on the existing four-node MITC4 element in OpenSees [35], Lu et al. [36] developed a multi-layered shell element, and verified that the model can simulate the complex mechanical behavior of shear walls well. In light of the shortcoming that the shell element cannot be directly connected with the beam column element, a high-performance quadrilateral flat shell element, NLDKGQ, was proposed and integrated into OpenSees [37]. In modeling the grid walls, ordinary concrete, EPS concrete and transverse distributed steel bars were modeled using the NLDKGQ element. The relative thickness of each layer was calculated based on the relative cross-sectional area of concrete, EPS concrete and transverse steel bars, generating the layered shell section of the grid shear wall, and the total thickness of section was the thickness of the grid shear wall. This section was then assigned to the layered shell element to complete the model definition. Figure 6 shows the

layered shell section. There were a total of ten layers along the thickness direction, where the transverse reinforcement was divided into two layers, the EPS concrete accounted for two layers, and the rest were layers of concrete.

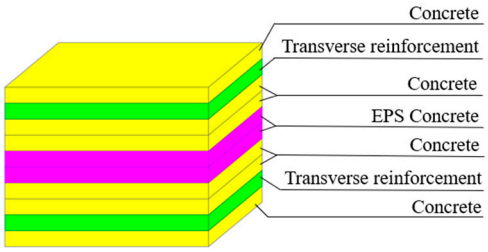

Figure 6. Sections of layered shell.

3.3. Material Constitutive Model

3.3.1. Constitutive Model of Concrete

The constitutive models of ordinary concrete and EPS concrete both used a multi-dimensional concrete material model proposed by Lu et al. [36]. The concrete material model was introduced to OpenSees through "nDMaterialPlaneStressUserMaterial" and "nDMaterial PlateForm Stress". The parameters are listed in Appendix A [36]. In the model, the main parameters were as follows. The compressive strengths (f_c) of the concrete and EPS concrete were 25.3 MPa and 0.32 MPa [33], respectively. The concrete tensile strength (f_t) was calculated as $f_t = 0.26 f_c^{2/3}$ based on the literature [38]. The crushing strength (f_{cu}) was taken as 20% of f_c according to the model developed by Kent and Park [39]. The concrete strain at peak strength (epsc0) was taken as −0.002. The concrete ultimate tensile strain (epstu) was 0.001. The shear transferring factor (stc) ranged from 0.05 to 0.08. The shear modulus was taken as 0.4 times of the elastic modulus [40].

3.3.2. Constitutive Model of Reinforcement

The constitutive model used for the steel bar was "Steel 02" in OpenSees, which was derived from the Menegotto–Pinto constitutive model [41]. Steel 02 is a constitutive model that can consider the effects of isotropic strain hardening and Bauschinger behavior. This model provides high computational efficiency and accurately represents the yield and hardening behaviors of steel bars during loading, aligning well with the results of quasi-static tests on steel bars.

The vertical reinforcement material used for the truss element "Steel02", and transverse reinforcement in the layered shell element required the addition of a multidimensional steel material model, "PlateRebar", to the steel02. The main parameters for reinforcement included the yield strength of steel F_y (F_y was set to 400 MPa), the elastic modulus E_0 (200,000 MPa), the strain hardening rate b (0.01) and the parameters R_0, cR_1 and cR_2, which controlled the curvature of the material during the elastic to elastoplastic transition, for which the recommended values were 18.5, 0.925 and 0.15, respectively.

3.4. Model Loading and Boundary Conditions

Unlike the load–displacement hybrid control loading scheme used in the experiment, the displacement loading method was used in the numerical simulation to control the horizontal loading displacement more accurately. Both specimens underwent displacement control, with identical displacement values applied. The displacement loading history is shown in Figure 7.

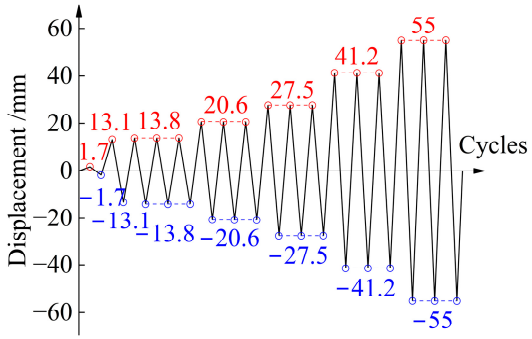

Figure 7. Loading history.

To accurately replicate the vertical and horizontal loads acting on the grid shear wall specimens during testing, a reference point was positioned at the midpoint of the upper boundary of the model. This reference point was coupled with all the nodes along the upper boundary, ensuring the uniformity of all degrees of freedom with the central reference point. Horizontal and vertical loads were applied at this reference point to simulate the horizontal displacement and vertical axial force of the grid shear wall specimen.

In order to replicate the experimental conditions, the ground beam was fully anchored to the ground, and the model was also fixed to the ground. All six degrees of freedom of each node at the base of the model were constrained, ensuring that the grid shear wall model remained rigidly connected to the ground without slippage. The finite element model and boundary conditions of specimen W1 are illustrated in Figure 8. It can be seen from Figure 8 that the truss element and shell element shared the same node.

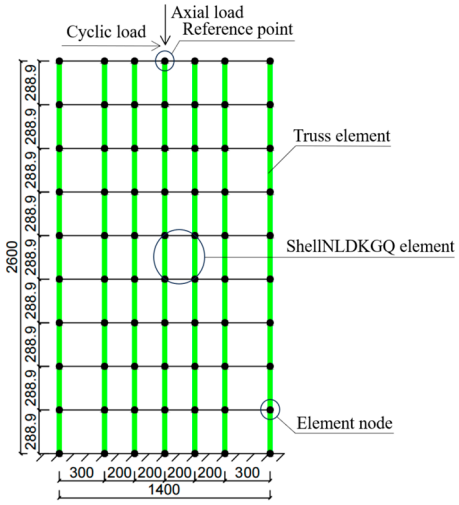

Figure 8. Finite element model diagram.

The static analysis was divided into two steps: a constant vertical load step and a lateral displacement step. After submitting the calculation, nonlinear finite element analyses of the specimens were carried out. The predicted lateral load versus top displacement curve was obtained by recording the displacements and forces of node at the reference point in Figure 8.

4. Validation of the Model

The comparison between the predicted hysteretic load versus top displacement curve and the experimentally measured response [33] of specimens W1 and W2 is shown in Figure 9, and the comparison of skeleton curves is presented in Figure 10. In these figures,

positive values of the curve indicate forward loading (pushing) of the specimen, while negative values represent reverse loading (pulling) of the specimen.

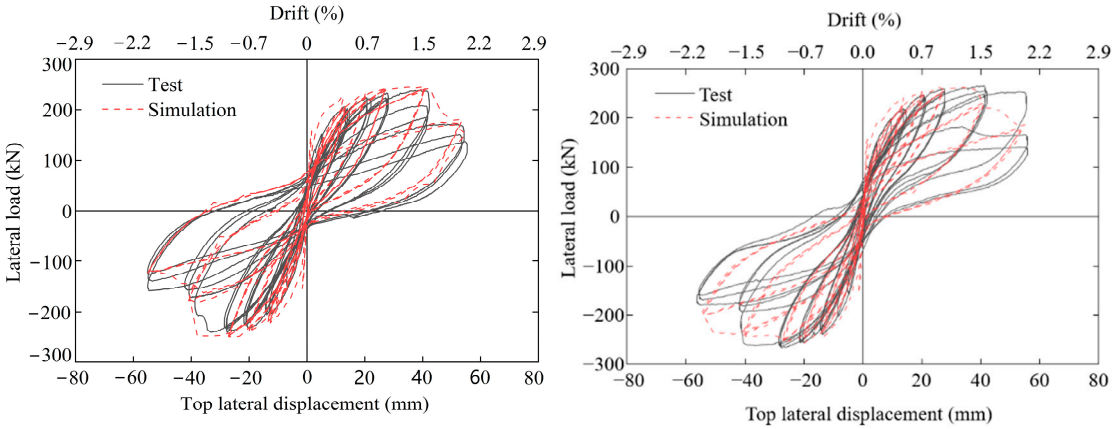

(**a**) W1 (**b**) W2

Figure 9. Comparison of hysteretic curves.

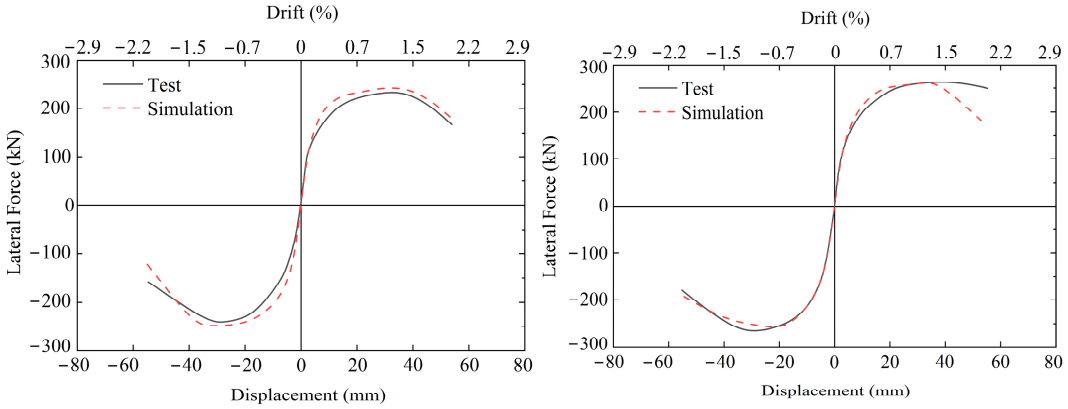

(**a**) W1 (**b**) W2

Figure 10. Comparison of skeleton curves.

From Figure 9, it is evident that the hysteresis loop of the simulation curve closely aligns with the test curve. The peak load, deformation capacity, stiffness degradation and the shape of the hysteretic loops and pinching behavior of the simulated curve are in good agreement with the experimental results, which indicates that the combined model of layered shell elements and truss elements can adequately describe the hysteretic characteristics of grid shear walls under a cyclic load.

It can be seen from Figure 10 that the combined model of layered shell elements and truss elements had high accuracy, and the maximum relative error for predicting the peak load of grid shear walls was within 5%. However, it is worth noting that the simulated lateral load of the skeleton curve of specimen W2 under positive loading decreased faster than that of the experimental curve after reaching the peak load. The main reasons for the error in the simulation analysis could be as follows: (1) The applied vertical load was difficult to maintain and decreased at the later loading period in the test, especially for specimen W2, but the constant value of the axial load was used in the simulation. (2) There were errors between the simplified material model and the real material.

5. Parameter Influence Analysis

On the basis of verifying the rationality of the calculation model of the grid shear wall, the influence of the main parameters on the seismic performance of the grid shear wall

was further studied. Generally speaking, the axial load ratio will affect the performance of shear walls, so the axial load ratio was selected to be one of the parameters. The grid shear wall was composed of vertical limbs and transverse limbs. The reinforcement ratio of the vertical limbs and transverse limbs, the length of the vertical limbs and the height of the transverse limbs are the main parameters that affect the seismic performance of grid shear walls. Since the length of the vertical limb was reflected in the specimens (110 mm and 210 mm), the reinforcement ratio of the vertical limbs and transverse limbs and the height of the transverse limb were selected for parameter analysis.

As the selected grid shear wall specimens were slender walls with a large aspect ratio, for this research, the parameter influence analysis was carried out on this basis. Grid shear walls with small shear span ratios were not in the scope of this study. Each parameter of the model was systematically modified while keeping others constant to analyze its individual effect. Utilizing specimen W1 as the baseline model for finite element parameter analysis, the influence of the above parameters on the seismic performance of grid shear walls was studied. Detailed values of the calculation parameters of different grid shear walls are presented in Table 2.

Table 2. Different grid shear walls for parameter analysis.

Parameter	Parameter Value				
Axial load ratio	0.05	0.15	0.1	0.2	0.3
Vertical reinforcement ratio	0.46%	0.71%	1.03%	1.40%	—
Transverse reinforcement ratio	0.25%	0.39%	0.57%	0.77%	—
Transverse limb height	100 mm	200 mm	300 mm	—	—

5.1. Axial Load Ratio

The axial load ratio, denoted as n_0, is defined as $n_0 = N/f_c A$, where N represents the axial load force, f_c signifies the design value of the concrete axial compressive strength, and A denotes the cross-sectional area of the grid shear wall after deducting the opening. Axial load ratio has a significant effect on the seismic performance of traditional RC shear walls, which affects their load capacity, ductility and energy dissipation capacity.

In order to investigate the effect of axial load ratio on the seismic performance of grid shear walls, the seismic behavior of grid shear walls under different axial load ratios is analyzed based on the W1 reference model (designed with an axial load ratio of 0.15). In the simulation, design axial load ratios of 0.05, 0.1, 0.2 and 0.3 were selected in this study, and other parameters were consistent with the benchmark model. The upper limit of the design axial load ratio was set to 0.3, mainly because grid shear walls are suitable for medium- and high-rise buildings with a building height below 40 m. The differences in load capacity and the predicted load versus displacement skeleton curves of grid shear walls under different axial load ratios are shown in Figure 11. Furthermore, Table 3 presents the peak load capacity of the grid shear walls under different axial load ratios.

From Figure 11 and Table 3, it is evident that the load–displacement curves of each grid shear wall followed a similar trend. Before yielding, the load–displacement curve of the wall remained linear, with a subsequent decrease in stiffness post-yield. The lateral load capacity consistently decreased with the increase in displacement. With the increase in the axial load ratio, the load capacity and lateral stiffness of the wall increased significantly, but the ductility decreased.

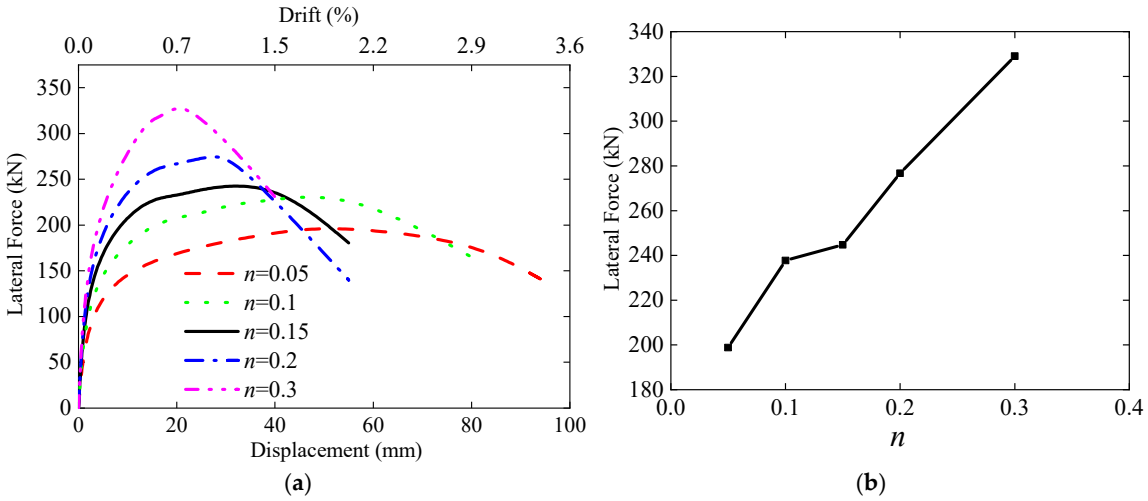

Figure 11. Influence of axial load ratio. (**a**) Lateral load–displacement skeleton curve. (**b**) Relationship between peak load and axial load ratio curve.

Table 3. Influence of axial load ratio on load capacity of grid shear walls.

Axial Load Ratio	Peak Load Capacity (kN)	Relative Value of Peak Load Capacity	Ultimate Drift Ratio	Relative Value of Ultimate Drift Ratio
0.05	198.8	0.81	1/33	1.52
0.1	237.7	0.97	1/41	1.22
0.15 (test specimen)	244.7	1	1/50	1
0.2	276.7	1.13	1/71	0.70
0.3	329.0	1.34	1/86	0.58

When the axial load ratio increased from 0.05 to 0.3, the skeleton curve of the grid shear wall changed significantly. The peak load capacity rose from 198.8 kN to 329.0 kN, with a 53% increase in the peak load capacity and a 94% decrease in the ultimate drift ratio. However, the ultimate drift ratio of all specimens exceeded 1/120, meeting the criteria for elastic–plastic deformation of shear wall structures under rare earthquakes required by code for the seismic design of buildings [42]. According to the calculation results, grid shear walls can be used for medium- and high-rise buildings with a height of less than 40 m.

5.2. Vertical Reinforcement Ratio

The vertical reinforcement ratio, denoted as ρ_v, represents the ratio of the cross-sectional area of vertical steel bars to the cross-sectional area of vertical limbs. To investigate the influence of the vertical steel reinforcement ratio on the seismic performance of grid shear walls, seismic behavior of grid shear walls with different vertical reinforcement ratios was examined by altering the vertical reinforcement ratio based on the W1 benchmark model (featuring a vertical reinforcement diameter of 10 mm). New models were created with vertical steel bar diameters of 8 mm, 12 mm and 14 mm, resulting in calculated vertical reinforcement ratios of 0.46%, 1.03% and 1.40%, respectively. According to the seismic design code [42], the minimum diameter of the vertical distribution of steel bars in traditional shear walls is 8 mm, the most commonly used diameters for steel bars are 8 mm and 10 mm, and the maximum diameter is 14 mm. Therefore, the reinforcement ratio of vertically distributed steel bars within the diameter range of common steel bars was calculated to ensure a reasonable vertical reinforcement ratio. The remaining parameters were kept consistent with the benchmark model. The differences in load capacity were compared, and the finite element analysis results of the walls under different vertical

reinforcement ratios are shown in Figure 12. Additionally, Table 4 presents the peak load capacity of the walls under different vertical reinforcement ratios.

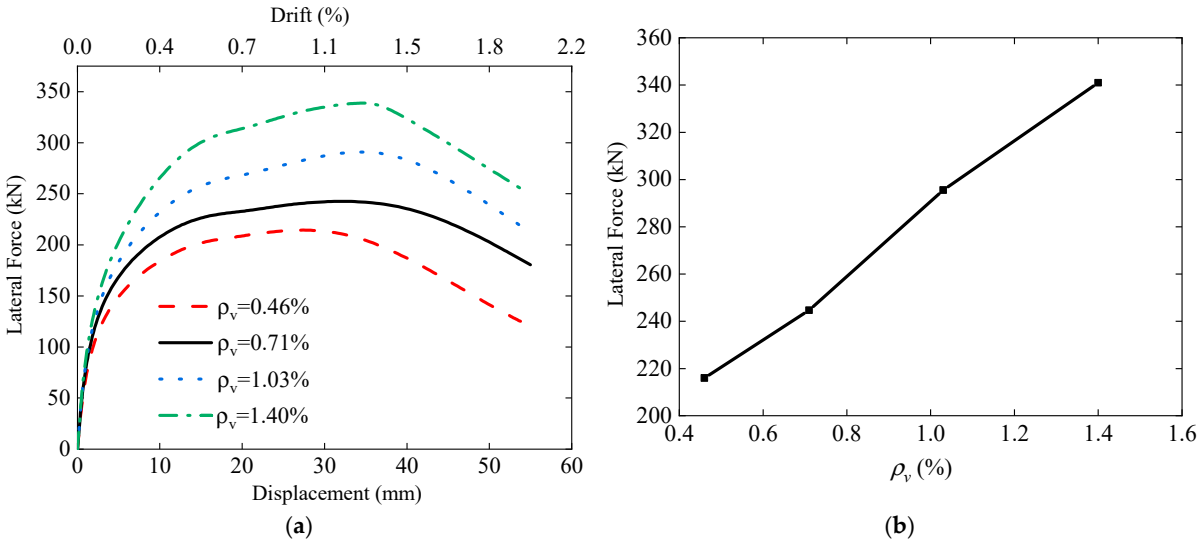

Figure 12. Influence of vertical reinforcement ratio. (**a**) Lateral load–displacement skeleton curve. (**b**) Relationship between peak load and vertical reinforcement ratio.

Table 4. Influence of vertical reinforcement ratio on load capacity.

Reinforcement Ratio (%)	Peak Load Capacity (kN)	Relative Value
0.46	216.0	0.88
0.71 (test specimen)	244.7	1
1.03	295.5	1.21
1.40	341.0	1.39

From Figure 12 and Table 4, it is evident that the load–displacement curves of the grid shear walls exhibited a similar trend. Augmenting the vertical steel reinforcement markedly improved the load capacity and lateral stiffness of the walls. Before reaching the peak load, the load capacity of each wall rapidly increased with lateral displacement. After the peak load, with the increase in displacement, the load capacity and stiffness of each wall decreased.

The vertical reinforcement ratio was increased from 0.46% to 1.40%, resulting in a noteworthy 51% increase in the peak load capacity of the grid shear wall. Moreover, there was a substantial improvement in the initial stiffness of the walls. The increase in vertical reinforcement ratio was beneficial, as it improved the seismic performance of the grid shear wall. Considering the cost and bearing capacity comprehensively, the suitable vertical steel bars in the vertical limb of the grid shear walls are 10 mm and 12 mm diameters. That is, the reinforcement ratio of the vertical limb is recommended to be 0.7–1.0%.

5.3. Transverse Reinforcement Ratio

The transverse reinforcement ratio, denoted as ρ_h, signifies the ratio of the cross-sectional area of the transverse steel bars to the cross-sectional area of the transverse limbs. To examine the influence of the transverse reinforcement ratio on the seismic performance of grid shear walls, new models with transverse reinforcement diameters of 8 mm, 12 mm and 14 mm were established based on the W1 benchmark model (featuring a transverse reinforcement diameter of 10 mm), resulting in calculated transverse reinforcement ratios of 0.25%, 0.57% and 0.77%, respectively. All other parameters remained consistent with the benchmark model. The differences in load capacity were compared, and the finite

element analysis results of grid shear walls with different transverse reinforcement ratios are presented in Figure 13. Furthermore, Table 5 illustrates the peak load capacity of the grid shear walls with different transverse reinforcement ratios.

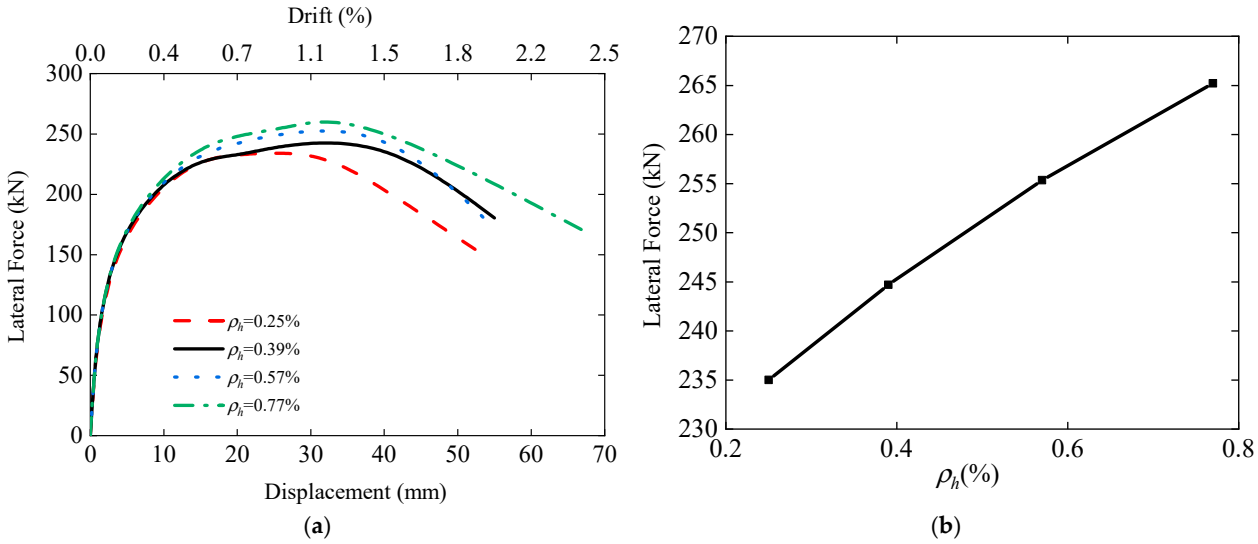

Figure 13. Influence of transverse reinforcement ratio. (**a**) Lateral load–displacement skeleton curve. (**b**) Relationship between peak load and transverse reinforcement ratio.

Table 5. Influence of transverse reinforcement ratio on load capacity.

Reinforcement Ratio (%)	Peak Load Capacity (kN)	Relative Value
0.25	235.0	0.96
0.39 (test specimen)	244.7	1
0.57	255.3	1.04
0.77	268.4	1.09

From Figure 13 and Table 5, it is apparent that the skeleton curves of each wall exhibited a similar trend. Before a drift ratio of 0.375% was reached, the skeleton curves essentially overlapped, indicating comparable initial stiffness across the walls. However, beyond this point, a noticeable disparity emerged in the lateral load of the skeleton curve with increasing horizontal displacement. Overall, this trend suggests that a higher transverse reinforcement ratio corresponds to a greater lateral load capacity. However, when the transverse reinforcement ratio increased from 0.25% to 0.77%, the peak load capacity of the grid shear wall only experienced a modest 13% increase. Notably, the peak load capacity of the grid shear wall featuring a transverse reinforcement ratio of 0.25% amounted to 96% of that of the benchmark model, indicating a marginal decrease. Conversely, the peak load capacity of the grid shear wall increased by 9% when the transverse reinforcement ratio was 0.77%, as compared to the benchmark model with transverse reinforcement ratio of 0.39%. This increase was accompanied by improved ductility. In summary, it seems that the transverse reinforcement ratio has a relatively minor impact on the load capacity of grid shear wall due to the fact that grid shear walls with large shear span ratios primarily experience bending failure. Therefore, for grid shear walls with large shear span ratios, the ratio of horizontal steel reinforcement in the transverse limb is about 0.25–0.4%.

5.4. Transverse Limb Height

To investigate the influence of transverse limb height on the seismic performance of grid shear walls, new models with transverse limb heights of 100 mm and 300 mm were established based on the W1 benchmark model (which features a cross-section height

of 200 mm). All other parameters remained consistent with the benchmark model. The difference in the load capacity of three walls was compared. The finite element analysis results of the grid shear walls under different transverse limb heights are shown in Figure 14, while the peak load capacity of the walls under different transverse limb heights is listed in Table 6.

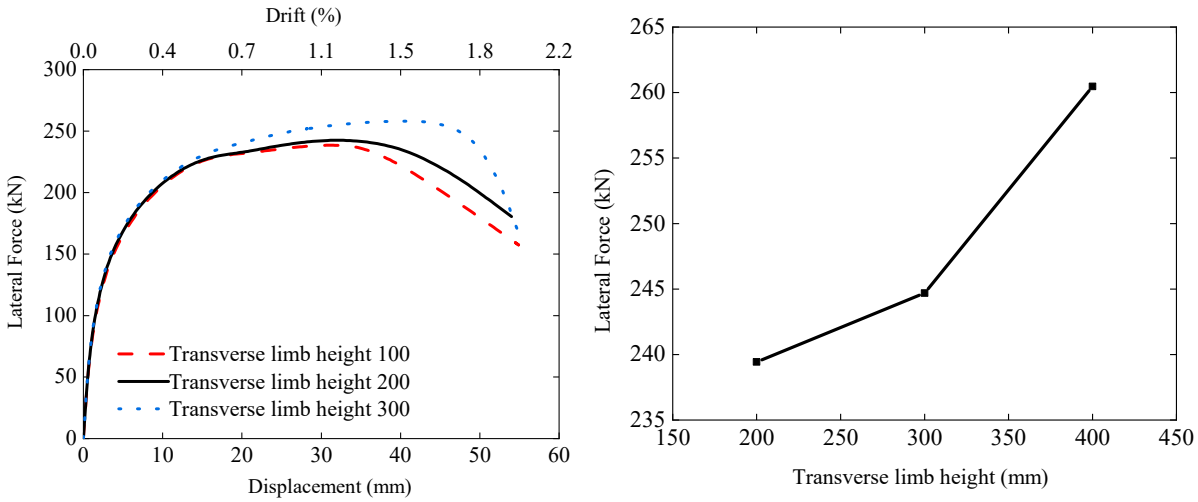

Figure 14. Influence of transverse limb height. (**a**) Lateral load–displacement skeleton curve. (**b**) Relationship between peak load and limb height.

Table 6. Influence of transverse limb height on load capacity.

Transverse Limb Height (mm)	Peak Load Capacity (kN)	Relative Value
100	239.4	0.98
200 (test specimen)	244.7	1
300	260.5	1.06

From Figure 14 and Table 6, it is evident that the skeleton curves of each wall exhibited a similar trend, essentially overlapping before a drift ratio of 0.4% was reached. At this point, the initial stiffness of each wall was basically the same. However, after a drift ratio of 0.4% was reached, the lateral load of the skeleton curve of the grid shear walls with transverse heights of 100 mm and 300 mm was significantly different with the increase in lateral displacement, indicating that the higher the transverse height, the greater the load capacity.

However, when the height of the transverse limb was increased from 100 mm to 300 mm, the peak load capacity of the grid shear wall only increased by 8%. For grid shear walls with large aspect ratios, the impact of the transverse height on the load capacity is relatively minimal. It should be noted that the load capacity of the grid shear wall with a transverse height of 300 mm diminished rapidly after reaching the peak load, indicating that the failure mode of the wall might have changed and that a large height of the transverse limb should be avoided. Therefore, it is recommended that the transverse limb height of the grid shear walls be 100–200 mm.

6. Conclusions

Through nonlinear finite element analysis of grid shear wall specimens, the reliability of the modeling approach for grid shear walls was verified. Based on this, the influence of parameters such as the axial load ratio, vertical reinforcement ratio, transverse reinforce-

ment ratio and transverse limb height on the seismic performance of grid shear walls was investigated. The main conclusions are as follows:

1. A new grid shear wall model combining truss elements and shell elements is proposed, and its modeling approach is introduced in detail. The simulated hysteresis curves agreed well with the experimental results, indicating that the proposed model of grid shear walls was accurate and reasonable.
2. The axial load ratio increased from 0.05 to 0.3, the peak load capacity increased by 53%, and the ultimate drift ratio decreased by 94%. This increase significantly improved the load capacity of the grid shear walls, but led to a decrease in deformation capacity. However, when the axial load ratio was 0.3, the ultimate drift ratio of the grid shear wall still met the elastic–plastic deformation criterion of shear wall structures under rare earthquakes, as required by Chinese code.
3. The vertical reinforcement ratio increased from 0.46% to 1.40%, resulting in a 51% increase in the peak load capacity. This increase significantly enhanced the load capacity of the grid shear walls. Conversely, transverse reinforcement ratio increased from 0.25% to 0.77%, leading to only a 13% increase in the peak load capacity. Increasing the transverse reinforcement ratio had a relatively minor effect on the load capacity of grid shear walls with flexure-dominated behavior. According to the simulation results, reasonable ratio of vertical reinforcement and transverse reinforcement of grid shear walls is proposed for medium- and high-rise buildings: reinforcement ratio of the vertical limb should be about 0.7~1.0%, and reinforcement ratio of the transverse limb should be about 0.25~0.4%.
4. Increasing the height of the transverse limb from 100 mm to 300 mm increased the peak load capacity by 8%. Increasing the transverse limb height had minimal effect on the load capacity of the grid shear wall, and a large height of the transverse limb should be avoided because of the reduced ductility. Therefore, the recommended height for the transverse limb of grid shear walls is 100–200 mm.

As the grid shear wall specimens selected in this study were all slender walls with large shear span ratios, the parameter influence analysis was only carried out on this basis. In the future, the method proposed in this research will be applied to grid shear walls with small span shear ratios for further parametric study.

Author Contributions: Conceptualization, W.Z.; methodology, W.Z. and C.L.; software, C.L.; validation, W.Z. and X.C.; formal analysis, C.L. and X.C.; investigation, W.Z.; resources, C.L. and X.C.; data curation, C.L. and X.C.; writing—original draft preparation, W.Z. and C.L.; writing—review and editing, W.Z.; visualization, W.Z.; supervision, W.Z.; project administration, W.Z.; funding acquisition, W.Z. All authors have read and agreed to the published version of the manuscript.

Funding: This work was supported by the National Natural Science Foundation of China (grant no. 52078012).

Data Availability Statement: The data presented in this study are available on request from the author.

Conflicts of Interest: The authors declare no conflicts of interest.

References

1. Aye, L.; Ngo, T.; Crawford, R.H.; Gammampilaa, R.; Mendis, P. Life cycle greenhouse gas emissions and energy analysis of prefabricated reusable building modules. *Energy Build.* **2012**, *47*, 159–168. [CrossRef]
2. Pungercar, V.; Zhan, Q.S.; Xiao, Y.Q.; Musso, F.; Dinkel, A.; Pflug, T. A new retrofitting strategy for the improvement of indoor environment quality and energy efficiency in residential buildings in temperate climate using prefabricated elements. *Energy Build.* **2021**, *241*, 110951. [CrossRef]

3. Chen, Y.J.; Kang, C.F.; Wu, Y.F.; Qian, Z.C. Bending Performance of Precast Ceramsite-Concrete-Insulated Sandwich Panel with Stainless Steel Shear Connectors. *Buildings* **2022**, *12*, 1640. [CrossRef]
4. Wang, Q.K.; Shen, C.X.; Guo, Z.; Zhu, K.; Zhang, J.J.; Huang, M. Research on the Barriers and Strategies to Promote Prefabricated Buildings in China. *Buildings* **2023**, *13*, 1200. [CrossRef]
5. Wang, Q.; Qian, J.R.; Ma, B.M.; Hu, Q.C.; Feng, B.C. Experimental study on seismic behavior of concrete grillage walls. *J. Build. Struct.* **2004**, *25*, 15–25. (In Chinese)
6. Zhang, W.J.; Du, Y.N.; Kang, H.Z.; Qian, J.R.; Feng, B.C. Experimental study on seismic behavior of large grid size RC shear walls. *J. Build. Struct.* **2011**, *32*, 116–124. (In Chinese)
7. Zhang, W.J.; Du, Y.N.; Qian, J.R. Experimental Research on Seismic Performance of Cast-In Situ RC Grillage Shear Walls Formed with Heat Preservation Hollow Blocks. *Adv. Mater. Res.* **2012**, *446*, 672–678.
8. Zhang, W.J.; Chu, X. Study on seismic behavior of grid shear wall with different grid spacing and small shear-span-ratio. *World Earthq. Eng.* **2023**, *39*, 89–99. (In Chinese)
9. Dusicka, P.; Kay, T. Seismic Evaluation of a Green Building Structural System: ICF Grid Walls. In *Structures Congress 2009: Don't Mess with Structural Engineers: Expanding Our Role*; American Society of Civil Engineers: Reston, VA, USA, 2009; pp. 1–7.
10. Dusicka, P.; Kay, T. In-plane lateral cyclic behavior of insulated concrete form grid walls. *J. Struct. Eng.* **2011**, *137*, 1075–1084. [CrossRef]
11. Asadi, P.; Madandoust, R.; Zahrai, S.M. Response modification factor due to ductility of screen-grid ICF wall system in high seismic risk zones. *KSCE J. Civ. Eng.* **2017**, *21*, 258–264. [CrossRef]
12. Lopez, A.; Bazaez, R.; Leiva, G.; Loyola, R.; Gomez, M. Experimental study of in-plane flexural behavior of screen-grid insulated concrete form rectangular and T-shaped walls. *Eng. Struct.* **2021**, *247*, 113128. [CrossRef]
13. Kolozvari, K.; Biscombe, L.; Dashti, F.; Dhakal, R.P.; Gogus, A.; Gullu, M.F.; Henry, R.C.; Massone, L.M.; Orakcal, D.; Rojas, F.; et al. State-of-the-art in nonlinear finite element modeling of isolated planar reinforced concrete walls. *Eng. Struct.* **2019**, *194*, 46–65. [CrossRef]
14. Chayaboot, K.; Boonpichetvong, M.; Pannachet, T.; Sata, V.; Chintanapakdee, C. Seismic Performance of Infilled Reinforced Concrete Frame with Crumb Rubber Mortar Wall Panel. *Civ. Eng. J.* **2024**, *10*, 468–488. [CrossRef]
15. Habieb, A.B.; Hidayat, M.R.; Sutrisno, W.; Kandymov, N.; Milani, G. Effectiveness of Different Configurations of Ferrocement Retrofitting for Seismic Protection of Confined Masonry: A Numerical Study. *Civ. Eng. J.* **2024**, *10*, 2781–2803. [CrossRef]
16. Xu, X.F.; Wang, T. Numerical Study on Precast RC Wall Panels with Angle Steel Boundary Components. *Appl. Mech. Mater.* **2013**, *351*, 578–582.
17. Wang, J.J.; Liu, C.; Fan, J.S.; Jerome, F.; Nie, X. Triaxial concrete constitutive model for simulation of composite plate shear wall–concrete encased: THUC3. *J. Struct. Eng.* **2019**, *145*, 04019088. [CrossRef]
18. Jothimani, V.T.; Guruswamy, S.V. Cyclic Performance of RC Shear Wall Embedded with X-Shaped Web Reinforcement. *Arab. J. Sci. Eng.* **2021**, *46*, 4971–4983. [CrossRef]
19. Zhang, W.J.; Yang, L.G.; Guo, X.T.; Li, A.Y.; Qian, J.R.; Zhang, Y.B. Experimental and numerical study on seismic performance of precast concrete hollow shear walls. *Eng. Struct.* **2023**, *291*, 116170. [CrossRef]
20. Mazzoni, S.; McKenna, F.; Scott, M.H.; Fenves, G.L. *OpenSees Users Manual*; Version 1.7.3; PEER; University of California: Berkeley, CA, USA, 2006.
21. Petracca, M.; Pelà, L.; Rossi, R.; Zaghi, S.; Camata, G.; Spacone, E. Micro-scale continuous and discrete numerical models for nonlinear analysis of masonry shear walls. *Constr. Build. Mater.* **2017**, *149*, 296–314. [CrossRef]
22. Olabi, M.N.; Caglar, N.; Kisa, M.H.; Yuksel, S.B. Numerical study on the response of composite shear walls with steel sheets under cyclic loading. *J. Build. Eng.* **2021**, *34*, 102069. [CrossRef]
23. Kolozvari, K.; Kalbasi, K.; Orakcal, K.; Wallace, J. Three-dimensional shear-flexure interaction model for analysis of non-planar reinforced concrete walls. *J. Build. Eng.* **2021**, *44*, 102946. [CrossRef]
24. Kolozvari, K.; Tran, T.A.; Orakcal, K.; Wallace, J. Modeling of cyclic shear-flexure interaction in reinforced concrete structural walls. II: Experimental validation. *J. Struct. Eng.* **2015**, *141*, 04014136. [CrossRef]
25. Kolozvari, K.; Kalbasi, K.; Orakcal, K.; Wallace, J. Three-dimensional model for nonlinear analysis of slender flanged reinforced concrete walls. *Eng. Struct.* **2021**, *236*, 112105. [CrossRef]
26. Zhang, W.J.; Li, Z.C. Design suggestions for special boundary elements of T-shaped shear walls. *Build. Struct.* **2024**, *54*, 78–85. (In Chinese)
27. Rojas, F.; Anderson, J.C.; Massone, L.M. A nonlinear quadrilateral thin flat layered shell element for the modeling of reinforced concrete wall structures. *Bull. Earthq. Eng.* **2019**, *17*, 6491–6513. [CrossRef]
28. Nakamura, N.; Tsunashima, N.; Nakano, T.; Tachibana, E. Analytical study on energy consumption and damage to cylindrical and I-shaped reinforced concrete shear walls subjected to cyclic loading. *Eng. Struct.* **2009**, *31*, 999–1009. [CrossRef]
29. Pozza, L.; Scotta, R.; Trutalli, D.; Pinna, M.; Polastri, A.; Bertoni, P. Experimental and numerical analyses of new massive wooden shear-wall systems. *Buildings* **2014**, *4*, 355–374. [CrossRef]

30. Alvarez, R.; Restrepo, J.I.; Panagiotou, M.; Santhakumar, A.R. Nonlinear cyclic Truss Model for analysis of reinforced concrete coupled structural walls. *Bull. Earthq. Eng.* **2019**, *17*, 6419–6436. [CrossRef]
31. Lu, Y.; Panagiotou, M.; Koutromanos, I. Three-dimensional beam-truss model for reinforced concrete walls and slabs–part 1, modeling approach, validation, and parametric study for individual reinforced concrete walls. *Earthq. Eng. Struct. Dyn.* **2016**, *45*, 1495–1513. [CrossRef]
32. Feng, D.C.; Xiong, C.Z.; Brunesi, E.; Parisi, F.; Wu, G. Numerical simulation and parametric analysis of precast concrete beam-slab assembly based on layered shell elements. *Buildings* **2020**, *11*, 7. [CrossRef]
33. Chu, X. *Study on Seismic Behavior of Reinforced Concrete Grid Shear Wall*; Beijing University of Technology: Beijing, China, 2022. (In Chinese)
34. Petracca, M.; Candeloro, F.; Camata, G. *STKO User Manual, Version 1.1*; ASDEA Software Technology: Pescara, Italy, 2017.
35. Dvorkin, E.N.; Bathe, K.J. A continuum mechanics based four-node shell element for general non-linear analysis. *Eng. Comput.* **1984**, *1*, 77–88. [CrossRef]
36. Lu, X.Z.; Xie, L.L.; Guan, H.; Huang, Y.L.; Lu, X. A shear wall element for nonlinear seismic analysis of super-tall buildings using OpenSees. *Finite Elem. Anal. Des.* **2015**, *98*, 14–25. [CrossRef]
37. Wang, L.S.; Cen, S.; Xie, L.L.; Lu, X.Z. Development of a shear wall model based on a new flat shell element for large deformation simulation and application in OpenSees. *Eng. Mech.* **2016**, *33*, 47–54. (In Chinese)
38. Teng, Z.M.; Luo, F.W.; Shi, L.Q. *Basic Components of Reinforced Concrete*; Tsinghua University Press: Beijing, China, 1987; pp. 14–15. (In Chinese)
39. Kent, D.C.; Park, R. Flexural members with confined concrete. *J. Struct. Div.* **1971**, *97*, 1969–1990. [CrossRef]
40. Shi, S.S. Shear strength, Modulus of rigidity and Young's modulus of concrete. *China Civ. Eng. J.* **1999**, *32*, 47–52. (In Chinese)
41. Menegotto, M.; Pinto, P.E. Method of analysis for cyclically loaded reinforced concrete frames including changes in geometry and non-elastic behavior of elements under combined normal forces and bending moment. In *IASBE Proceedings*; IASB: London, UK, 1973; pp. 15–22.
42. *GB 50011-2010*; Code for Seismic Design of Buildings. China Architecture & Building Press: Beijing, China, 2016. (In Chinese)